Neurobiology of Disease

Progressive Supranuclear Palsy PERK Haplotype B Selectively Translates DLX1 Promoting Tau Toxicity

Christian B. Lessard,[1,2,3] Diego Rubio Rubio,[1,2,3] Samantha Tolton,[4] Marangelie Criado-Marrero,[1,2,3] Sakthivel Ravi,[1,2,3] Tristyn N. Garza,[1,2,3,5] John Koren,[1,2,3] Jennifer Philips,[1,6,7] Pritha Bagchi,[8] Karen McFarland,[9] Deepak Chhangani,[10] Todd E. Golde,[9] Benoit I. Giasson,[1,2,3] Jada Lewis,[1,2,3,11] Paramita Chakrabarty,[1,2,3] Matthew J. LaVoie,[1,3,7,10] David R. Borchelt,[1,2,3] Nicholas T. Seyfried,[8] Stefan Prokop,[1,3,6,7] Diego E. Rincon-Limas,[1,2,3,10] and Jose F. Abisambra[1,2,3,5,12,13]

[1]Center for Translational Research in Neurodegenerative Disease, College of Medicine, University of Florida, Gainesville, Florida 32610, [2]Department of Neuroscience, University of Florida, Gainesville, Florida 32610, [3]Evelyn F. and William L. McKnight Brain Institute, University of Florida, Gainesville, Florida 32610, [4]Department of Biochemistry & Cell Biology, Boston University Chobanian & Avedisian School of Medicine, Boston, Massachusetts 02215, [5]Genetics Institute, University of Florida, Gainesville, Florida 32610, [6]Department of Pathology, University of Florida, Gainesville, Florida 32610, [7]Normal Fixel Institute for Neurological Diseases, University of Florida, Gainesville, Florida 32610, Departments of [8]Biochemistry and [9]Pharmacology and Chemical Biology, Emory School of Medicine, Atlanta, Georgia 30322, [10]Department of Neurology, University of Florida, Gainesville, Florida 32610, [11]Department of Physiological Sciences, College of Veterinary Medicine, Gainesville, Florida 32610, [12]Brain Injury Rehabilitation and Neuroresilience (BRAIN) Center, University of Florida, Gainesville, Florida 32610, and [13]Brain Rehabilitation Research Center, Malcom Randall VA Medical Center, North Florida/South Georgia Veterans Health System, Gainesville, Florida 32608

The unfolded protein response (UPR) sensor PERK exists in haplotypes A and B. PERK-B confers increased risk for tauopathies like progressive supranuclear palsy (PSP), but the mechanisms distinguishing its function from PERK-A and contributing to its association with tauopathy remain unknown. Here, we developed a controlled cellular model for a pair-wise comparison of the two PERK haplotypes, finding their UPR functions nearly indistinguishable. Puromycin-based proteomics highlighted a subset of mRNA translation events that was permissible under the PERK-B–dependent, but not the PERK-A–dependent, UPR. One of the targets that escaped PERK-B suppression was the transcription factor DLX1, which is genetically linked to PSP risk. We found that DLX1 solubility shifted to a detergent-insoluble fraction in the human brain tissue from male and female PSP donors. Furthermore, silencing the fly homolog of DLX1 was sufficient to decrease tau-induced toxicity in vivo. Our results detail the haplotype-specific PERK-B/DLX-1 pathway as a novel driver of tau pathology in cells, flies, and likely the human brain, revealing new insights into PSP pathogenesis and potential therapeutic targets.

Key words: **Alzheimer's disease; DLX1; PERK; progressive supranuclear palsy; tau**

Significance Statement

Progressive supranuclear palsy (PSP) is a devastating neurodegenerative tauopathy with no effective treatments. This study identifies how a genetic risk factor for PSP, the PERK-B haplotype, contributes to disease pathogenesis. Using novel cellular and animal models, we demonstrate that PERK-B selectively promotes translation of DLX1, a transcription factor genetically linked to PSP. Importantly, DLX1 accumulates in a detergent-insoluble fraction in human PSP brains, and reducing DLX1 mitigates tau-induced toxicity in vivo. These findings reveal a previously unknown PERK-B/DLX1 pathway that drives tauopathy. Our work opens new avenues for therapeutic intervention in PSP and related tauopathies. More broadly, this research highlights the importance of haplotype-specific effects and selective translational regulation in neurodegenerative disease, with implications for personalized medicine approaches.

Received Sept. 5, 2025; revised Dec. 29, 2025; accepted Feb. 6, 2026.

Author contributions: C.B.L., D.R.R., M.C.-M., S.R., J.K., T.E.G., B.I.G., J.L., P.C., M.J.L., D.R.B., D.E.R.-L., and J.A. designed research; C.B.L., D.R.R., S.T., P.B., K.M., D.C., and D.E.R.-L. performed research; J.P., B.I.G., S.P., and D.E.R.-L. contributed unpublished reagents/analytic tools; C.B.L., D.R.R., S.T., M.C.-M., S.R., T.N.G., J.P., P.B., K.M., D.C., N.T.S., S.P., D.E.R.-L., and J.F.A. analyzed data; D.R.B. and J.F.A. wrote the paper.

This work was in part supported by the National Institutes of Health/National Institute on Aging (J.F.A. R01AG075900, J.F.A. R01AG074584, J.F.A. R21AG093972, D.E.R.-L. R01AG077534), National Institute for Neurological Disorders and Stroke (J.F.A. R01NS091329), the Alzheimer's Association (J.F.A. AARG-D-21-847204), and the Rotary Club (J.F.A. Coins for Alzheimer's Research Trust). The UF Neuromedicine Human Brain and Tissue Bank is supported by the Center for Translational Research in Neurodegenerative Diseases, the Evelyn F. and William L. McKnight Brain Institute and the 1Florida ADRC (NIH/NIA P30AG066506). We are grateful for Dr. Chad Dickey's early work on tau and PERK, which is the foundation of this line of research. We are also grateful for Dr. Peter Davies' instrumental work in the development of the PHF1 antibody used in these experiments. S.P. is the Charlotte and Howard Zimmerman Rising Star Professor with the Norman Fixel Institute for Neurological Diseases.

The authors declare no competing financial interests.

Correspondence should be addressed to Jose F. Abisambra at j.abisambra@ufl.edu.

This paper contains supplemental material available at: https://doi.org/10.1523/JNEUROSCI.1727-25.2026

https://doi.org/10.1523/JNEUROSCI.1727-25.2026

Introduction

Cells undergoing endoplasmic reticulum (ER) stress activate an adaptive tripartite mechanism called the unfolded protein response (UPR). The protein kinase ER-like kinase (PERK) pathway of the UPR attenuates translation by phosphorylating and thereby inhibiting the eukaryotic initiation factor 2α (eIF2α; Harding et al., 2000a; Marciniak et al., 2006). While phosphorylated eIF2α broadly suppresses translation, it selectively permits translation of transcription factors such as ATF4, which promotes expression of proteins that restore ER function. Therefore, in response to ER stress, PERK regulates both transcription and translation (Kaufman, 2002; Weihl et al., 2006). Failure to resolve ER stress, accompanied by long-term PERK activation, can lead to broad and sustained inhibition of protein synthesis and, ultimately, cell death (Wang et al., 1998).

Given that neuronal function requires de novo protein synthesis, long-term attenuation of translation is problematic, especially for neurons (Moreno et al., 2012; Koren et al., 2021). Maladaptive PERK activity leads to sustained suppression of translation and is deleterious for brain health. For example, PERK haploinsufficiency results in Wolcott–Rallison syndrome, which features developmental brain abnormalities (Aldrian et al., 2024). Consistent with the pathologic effects of PERK deficiency, PERK haplotype B (PERK-B) produces a hypomorphic PERK variant compared with haplotype A (PERK-A), and it is associated with higher risk of developing tauopathies such as progressive supranuclear palsy (PSP) and Alzheimer's disease (AD; Hoglinger et al., 2011; Liu et al., 2013; Ferrari et al., 2014; Bruch et al., 2017; Yuan et al., 2018). However, the mechanisms by which PERK-B contributes to tauopathy remain unknown. Association of an intronic sequence in PERK defining the haplotype B (PERK-B) with risk for PSP was identified in a GWAS (Hoglinger et al., 2011). Future studies identified that the intronic sequence was linked with three exonic polymorphisms: S136C (ER lumen), R166Q (ER lumen), and S704A (cytosolic; Liu et al., 2013; Ferrari et al., 2014; Bruch et al., 2017; Yuan et al., 2018).

Besides the genetic link, PERK is also implicated in tauopathies. Pathologically, active PERK (phosphorylated or pPERK) accumulates in pretangle neurons of tauopathy brains, including PSP, AD, Down syndrome, and frontotemporal dementia–tau (Hoozemans et al., 2009; Nijholt et al., 2012; Stutzbach et al., 2013; Lanzillotta et al., 2018, 2020). Moreover, accumulation of pathological tau drives chronic PERK activation without resolution of ER stress, further hampering neuronal function (Abisambra et al., 2013). While modifying PERK activity ameliorates accumulation of pathological tau, whether activating or inhibiting PERK confers benefits remains unclear (Moreno et al., 2013; Bruch et al., 2017; Yuan et al., 2018; Koren et al., 2021).

To define the enigmatic mechanism by which PERK drives diverging cell fates, we developed novel tools to specifically activate PERK-A and PERK-B and found no differences in their canonical functions. Using puromycin proteomics, we established translatomes of both PERK haplotypes, and the overwhelming number of translational targets was equally suppressed by both PERK-A and PERK-B. Critically, the expression of a small subset of proteins was uniquely preserved under PERK-B–induced ER stress that was not present with PERK-A. Among these novel targets was DLX1, a gene product strongly associated with PSP (Weber et al., 2018). These data reveal a novel pathway linking PERK function and genetic risk of PSP with mechanisms underlying the deposition of tau in cellular and *Drosophila* models of disease.

Materials and Methods

Antibodies. PERK was detected with D11A8 rabbit (Cell Signaling Technology #5683) or Anti-FLAG M2 (Sigma-Aldrich, F1804) antibodies. Tau was detected with rabbit antibody 3026 that was raised against recombinant 0N3R human tau (Strang et al., 2017). β-Actin was detected with AC-15 (Santa Cruz Biotechnology, sc-69879). Anti-puromycin antibody (clone 12D10) was purchased from EMD Millipore (#MABE343). Histone H3 antibody (#9715), pTau S202 (D4H7E; #39357), and p-eIF2α (Ser51, #9721) were purchased from Cell Signaling Technology. Total p-eIF2α (D3: sc-133132) and pTau S262 (sc-32828) were purchased from Santa Cruz Biotechnology. PHF1 antibody, originally generated by Dr. Peter Davies, was provided by Albert Einstein College of Medicine. Dlx1 antibody was purchased from Novus Biologicals (#16178). Secondary antibodies used for Western blots IRDye 800CW (#926-32212) were purchased from LI-COR Biosciences and Alexa Fluor 680 rabbit (#A-21109) from Thermo Fisher Scientific.

Plasmids. All plasmids used in this study were approved by the Environmental Health and Safety Office at the University of Florida. The human PERK haplotype A plasmid was obtained from Origene (#RC214993). Mutations corresponding to PERK haplotype B (S136C, R166G, and S704A), as previously described (Yuan et al., 2018), as well as the K622R mutation, were introduced into PERK-A by PCR-based mutagenesis and confirmed by DNA sequencing. The plasmids encoding ATF4-mScarlet-NLS (Addgene #115969) and pLVX-XBP1-mNeonGreen-NLS (Addgene #115968) were gifts from Dr. David Andrews (Nougarede et al., 2018). Human 0N4R tau was cloned into pcDNA3.1. The double mutant tau construct ("2X-TAU", 0N4R P301L/S320F) was digested with *BlpI* and *NheI*, and the tau fragment was subcloned into the 0N4R tau backbone. An alternative open reading frame (AltORF) strategy previously described (Vanderperre et al., 2013) was used to enable expression of a second protein in the +3 reading frame of EGFP. To generate this construct, we subcloned mApple fluorescent protein into pENTRY-EGFP using the *XhoI* restriction site, positioned C-terminally after the EGFP stop codon in the +3 reading frame. The correct insertion and reading frame of mApple were verified by DNA sequencing.

Cell lines and generation of HEK293T PERK knock-out cells. HEK293T cells were grown in DMEM supplemented with Corning 10% fetal bovine serum (GE) and 100 units/ml penicillin, 100 µg/ml streptomycin (Life Technologies). PERK knock-out (KO) HEK293T-cell line was generated with CRISPR/Cas9 genome editing (Ran et al., 2013). An RNA guide aiming exon 3 of PERK (sense CACCGTTTCCATGCTTTCACGGTCT and antisense AAACAGACCGTGAAAGCATGGAAAC) was subcloned in pSpCas9(BB)-2A-GFP (gift from Feng Zhang, Addgene #48138). Plasmid expressing the cloned gRNA was confirmed by sequencing and transfecting in HEK293T. Transfected cells were plated on 96-well plates, and single clones were analyzed for endogenous PERK expression level by Western blotting. Genomic DNA from colonies of interest was extracted for PCR analysis with the following primers (forward primer GCTCTTAATTACTATTATTC, reverse primer GATTGCAAAATAATGTATAA). PCR products were cloned in TOPO-TA (Thermo Fisher Scientific, #4500781). Cells were transiently transfected using calcium phosphate DNA-precipitation method (Waxman and Giasson, 2010). We used pcDNA3.1 as DNA carrier for small amount of transfected PERK. SH-SY5Y (ATCC) were maintained in Eagle's Minimum Essential Medium:F12 Medium 1:1(Invitrogen #11320-033), 10% FBS (Corning), and 1% penicillin/streptomycin (Life Technologies). The cells were transfected with Lipofectamine 3000 (Thermo Fisher Scientific) according to the manufacturer's recommendation with the following modifications. SH-SY5Y cells were transfected in a six-well plate with 3.75 µl of Lipofectamine reagent and 2 µg of total of DNA. The Lipofectamine–DNA mixture was incubated with the cells for 4 h, and fresh media were added. The cells were lysed 48 h later in the same conditions as previously mentioned.

Western blotting. Protein extracts were mixed 1:1 with 4× protein loading buffer (31.25 mM Tris–HCl, 2% LDS, 10% glycerol, 1.5%

β-mercaptoethanol, and Orange G), pH 7.5, and then electrophoretically separated on 12–4% Bis–Tris precast gels or 4–12% Tris–glycine gels (Bio-Rad Laboratories) as previously described (Meier et al., 2016; Koren et al., 2019b). Proteins were electrophoretically transferred onto Immobilon-PSQ PVDF membranes (Millipore Sigma, #ISEQ00010) and subsequently blocked in Tris-buffered saline (TBS) containing 0.5% casein for 3 h at room temperature. Primary antibodies were diluted in TBS with 0.2% Tween 20 (TBS-T) and incubated for 1 h at room temperature or overnight at 4°C. Membranes were washed three times (5 min each) in TBS-T, followed by a 1 h incubation with secondary antibodies diluted in TBS-T. After three additional 5 min washes in TBS-T, membranes were imaged using the Odyssey Infrared Imaging System (LI-COR). Biochemical cellular fractionation of 2X-TAU was performed as previously described (Goodwin et al., 2021).

Puromycin assay. Transfected cells were incubated with puromycin (10 μg/ml; 18.36 μM) for 1 h to label nascent peptides as previously described (Meier et al., 2016; Koren et al., 2019a). Following incubation, cells were lysed in RIPA buffer supplemented with EDTA-free protease inhibitor cocktail (Sigma-Aldrich) and 1 mM PMSF (Sigma-Aldrich). Lysates were sonicated and then centrifuged at 13,000 rpm for 15 min at 4°C. The resulting supernatants were collected, and protein concentrations were determined before analysis by Western blotting.

RNA extraction and RT-PCR. Total RNA was extracted from transfected cells using TRIzol reagent (Invitrogen), following the manufacturer's instructions. Reverse transcription (RT) was performed using the High-Capacity cDNA Reverse Transcription Kit (Thermo Fisher Scientific), with random primers for general transcript analysis and oligo-dT primers for specific detection of XBP1 mRNA splicing. Subsequent PCR amplification was carried out using Taq 2X Master Mix [New England Biolabs (NEB), #M0270] and gene-specific primers. Tau mRNA was amplified using a forward primer targeting an internal tau sequence (5′-GCAAATAGTCTACAAACCAGTTG-3′) and a reverse primer (5′-TAGAAGGCACAGTCGAGG-3′) complementary to the BGH polyadenylation sequence in the plasmid, ensuring detection of only the exogenous tau transcript. XBP1 was amplified with primers: forward (5′-AGAACCAGGAGTTAAGACAGC-3′) and reverse (5′-AGTCAATACCGCCAGAATCC-3′). GAPDH was amplified as a control using validated primers from Origene (catalog #HP205798).

RNA sequencing and data analysis. PERK constructs were transfected into PERK KO HEK293T cells, and total RNA was extracted 48 h post-transfection using TRIzol reagent (Invitrogen), following the manufacturer's protocol. Total RNA sequencing and bioinformatic analysis were performed by LC Sciences. Differential gene expression analysis was conducted, and significantly regulated genes were identified using a false discovery rate (FDR) threshold of $q < 0.05$. The resulting dataset was analyzed in R, and heatmaps were generated using the pheatmap package (Kolde, 2018; pheatmap, Pretty Heatmaps; R package version 1.0.12, https://github.com/raivokolde/pheatmap) to visualize expression patterns of differentially expressed genes.

Puromycin proteomics. As previously performed (Schmidt et al., 2009; Koren et al., 2019a,b), transfected cells expressing PERK constructs were incubated with puromycin (10 μg/ml; 18.36 μM) for 1 h, except for the negative control group, which was used to distinguish specific puromycinylated peptides from background or nonspecific proteins bound to the antibody–Dynabeads complex. Following treatment, cells were washed with PBS and lysed in a buffer containing 150 mM KCl, 10 mM $MgCl_2$, 5 mM HEPES, pH 7.4, and 1% Igepal CA-630, supplemented with EDTA-free protease inhibitor cocktail (Sigma-Aldrich) and 1 mM PMSF (Sigma-Aldrich). In parallel, 5 μg of anti-puromycin antibody was cross-linked to Dynabeads Protein G (NEB, #S1430S) following the manufacturer's protocol and as previously described (Koren et al., 2019a). Cell lysates were clarified by centrifugation at $16{,}000 \times g$ for 15 min at 4°C and then incubated with the antibody cross-linked Dynabeads for 16 h at 4°C on a rotator. After incubation, the immunoprecipitated complexes were washed three times with PBS containing 0.2% Tween 20, followed by additional washes with a larger volume of PBS to remove residual detergent. The bound puromycinylated nascent peptides were subsequently analyzed by mass spectrometry at Emory University.

Mass spectrometry data analysis. Raw mass spectrometry data were processed as previously described with minor adjustments (Meier et al., 2015, 2016). The resulting MaxQuant output files were imported into Perseus for initial filtering. Data were then exported to Excel for further statistical analysis in R, due to the large dataset size. Peptides were initially filtered to retain only those with at least three positive intensity values in one experimental group. For entries with two positive and one missing or null value, a permutation step was applied by replacing the missing value with the average of the two available values. Peptide detection was assessed relative to the negative control group. A peptide was considered positively detected if it showed a measurable intensity signal while the corresponding control value was zero. Conversely, peptides were classified as not detected if their average intensity in the experimental group was equal to or lower than the average intensity in the negative control. Statistical comparisons between each experimental group and the negative control were performed using one-tailed *t* tests, with test selection based on variance equality (Student's *t* test for equal variance, Welch's *t* test for unequal variance). Peptides with a significantly higher mean intensity ($p < 0.05$) compared with the negative control were classified as positively detected. Subsequently, two-tailed *t* tests were conducted to assess differences between experimental groups.

Gene ontology and data visualization. Gene ontology (GO) enrichment analysis was performed using g:Profiler (Kolberg et al., 2023) to identify biological processes associated with peptides uniquely detected in each experimental group. Venn diagrams were generated in R using the ggVennDiagram package (Gao and Dusa, 2024; ggVennDiagram, A "ggplot2" Implement of Venn Diagram; R package version 1.5.3; available at https://gaospecial.github.io/ggVennDiagram/, https://github.com/gaospecial/ggVennDiagram). Heatmaps were created using the pheatmap package (Kolde, 2018; pheatmap, Pretty Heatmaps; R package version 1.0.12; available at https://github.com/raivokolde/pheatmap) to visualize *Z*-scores of differentially detected peptides.

Drosophila *genetics and expression analysis. Drosophila* stocks for the eye-specific driver Gmr-Gal4 (B-1104), UAS-Luciferase RNAi control (B-31603), and RU-486–inducible mushroom body GeneSwitch Gal4 driver (MB-GS-Gal4; B-81013) were obtained from the Bloomington Drosophila Stock Center in Indiana, whereas the *Dll* RNAi line (v101750) was purchased from the Vienna Drosophila Resource Center. UAS transgenic flies expressing the longest human wild-type tau isoform (2N4R) as well as flies expressing human $A\beta_{42}$ fused to a secretory signal peptide were previously described (Casas-Tinto et al., 2011; Minjarez et al., 2016). For the experiments, we collected virgin flies from recombinant stocks carrying Gmr-Gal4, UAS-$A\beta_{42}$/Cyo and Gmr-Gal4, UAS-Tau/Cyo and crossed them with males from UAS lines expressing Luciferase RNAi or *Dll* RNAi transgenes. All the crosses were cultured on premade molasses-based food from Archon Scientific at 26°C. Eye phenotypes from progenies were documented using a Leica Z16 APO macroscope as described (Minjarez et al., 2016). Quantifications were performed using NIH ImageJ's measure tool and Flynotyper plugin to calculate differences in size and organization of the fly eyes, respectively. For *Dll* knock-down quantification, RNA was isolated from 20 fly heads expressing the recombinant GMR-Gal4, Tau/CyO with the Luciferase RNAi or *Dll* RNAi transgenes using Trizol (Invitrogen). RNA extracts were digested with TURBO DNAse (Ambion Life Technologies AM2238) for genomic DNA removal followed by phenol–chloroform cleaning. RT was performed with random primers as described by the provider (Thermo Fisher Scientific #4368814). Quantitative PCR was performed with SYBR (Power SYBR Green PCR Master Mix Life Technologies) with the following primers for GAPDH and *Dll* (GAPDH, F-gtctccaccgacttcttcag, R-acttgatcaggtc gatgacg; Dll, F-ggagcacctatcagcatttcg, R-cgcacttatcggagatggaga). RT products were diluted to ensure primer amplification near 100% and the Livak method was used to calculate the relative gene expression. At the

end of the cycle, the qPCR amplicons were loaded on an agarose gel to verify a single band at the appropriate molecular weight. For expression analysis in mushroom body neurons of the fly brain, female flies carrying the conditional MB-GS-Gal4 driver with tau were crossed with males bearing Luc RNAi or *Dll* RNAi transgenes. Progenies were collected upon eclosion and treated with RU-486 (100 µg/ml) for 5 d. Twenty fly heads per genotype were collected and subjected to Western blot as described above.

Statistical analysis. Statistics were performed with GraphPad Prism (USA) version 9.4. All data are expressed as the mean ± SEM or ±SD as described.

Large language model use. ChatGPT and Claude.AI were used to generate suggestions for the title, abstract, and the significance statement.

Results

PERK overexpression model

To examine the impact of PERK haplotypes A and B individually and independently of endogenous PERK expression, we generated a PERK KO human embryonic kidney (PERK KO HEK) cell line using a CRISPR/Cas9 strategy. We also produced plasmid constructs of PERK-A, PERK -B, and PERK-K (an enzymatically dead PERK variant, K622R, used as a negative control). Experimentally, ER stress is commonly induced with chemical compounds (e.g., thapsigargin and tunicamycin) that promote en masse calcium efflux from the ER (da Silva et al., 2020). To bypass confounds of chemically induced excitotoxicity, we transfected cells with varying amounts of plasmids expressing PERK-A, PERK-B, or PERK-K in PERK KO HEK cells for 48 h (Fig. 1*A*). We found that transient transfection with 100 ng of PERK variants was not toxic and induced PERK activation (Fig. 1*A*,*B*).

PERK haplotypes share common pathways and have similar effects on translation

We used ATF4 and Xbp1 sensors to determine the effect of PERK haplotypes on the PERK and Ire1 branches of the UPR in real time (Fig. 2*A*). ATF4-sensor fluorescence increased when either PERK-A or PERK-B was expressed (Fig. 2*B*); as expected, PERK-K failed to induce ATF4 fluorescence. As a positive control, chemical activation of the UPR with thapsigargin in PERK-A expressing cells induced ATF4 (Fig. 2*B*). PERK-A and PERK-B expression also activated the Ire1 pathway as evidenced by increased Xbp1 sensor fluorescence (Fig. 2*C*); interestingly, PERK-K also activated Xbp1, suggesting that PERK overexpression induces Ire1 independently of pPERK upregulation (Fig. 2*C*).

Given that active PERK (pPERK) was detected in PERK-A–overexpressing and PERK-B–overexpressing cells, we hypothesized that both PERK variants suppressed translation. To test this, we performed surface sensing of translation (SUnSET), a method that uses puromycin to label nascent proteins (Schmidt et al., 2009). PERK-A and PERK-B expression reduced puromycinylated proteins, and the decrease was similar in both conditions (Fig. 2*D*,*E*). Furthermore, we performed live-cell imaging and found that GFP levels, which served as a surrogate of protein synthesis, were significantly reduced by PERK-A and PERK-B, but not PERK-K; likewise, both PERK-A and PERK-B equally reduced GFP signal (Fig. 2*F*). PERK-A overexpression in combination with a PERK inhibitor (GSK2606414) rescued GFP fluorescence (Fig. 2*F*).

PERK reduces cap-dependent translation (Bell et al., 2016). To determine whether PERK-B reduced translation following the same mechanism, we generated a construct that measures cap-dependent translation by GFP expression; using the same construct in a different frame produces red (apple) fluorescence, which represents cap-independent translation (Fig. 2*G*). Similar to PERK-A, PERK-B reduced translation in a cap-dependent manner (Fig. 2*H–J*). As expected, neither construct reduced cap-independent translation.

PERK haplotypes differentially impact the levels and aggregation of pathological tau species

Given that PERK-B confers increased risk for tauopathies, we compared the effects of PERK-A and PERK-B on tau stability. We created a dose- and time-dependent window of PERK expression by transfecting 100 ng of PERK expression plasmids for 16 h. In this acute time frame, both PERK-A and PERK-B induced eIF2α phosphorylation compared with both the empty vector and PERK-K controls (Fig. S1). We then transfected 50 or 100 ng of PERK expression plasmids for 48 h (Fig. 3). We found that total PERK-A and PERK-B levels were increased in every condition; consistent with previous studies concluding that it is a hypomorph, PERK-B failed to produce significantly increased pPERK between 50 and 100 ng of plasmid (Fig. 3*A*,*B*). Interestingly, after 48 h, neither 50 nor 100 ng conditions showed detectable eIF2α phosphorylation beyond controls (Fig. 3*C*).

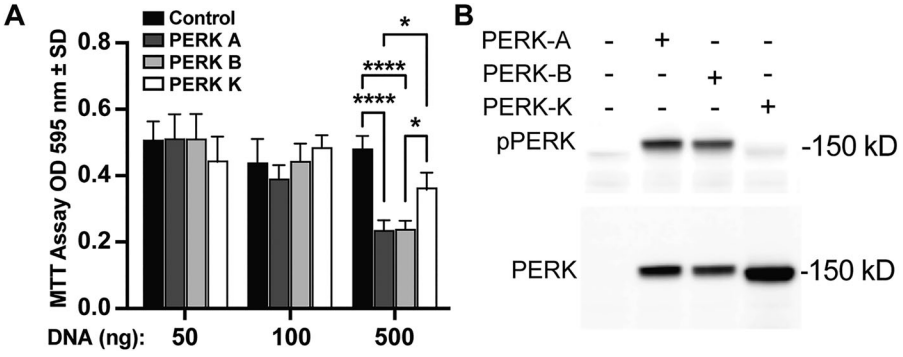

Figure 1. Mild PERK-A and PERK-B overexpression preserves cell viability while activating PERK. PERK KO HEK293T cells were transfected with varying low (nanogram) amounts of mammalian expression plasmids encoding PERK-A, PERK-B, PERK-K, or an empty plasmid used as a carrier control. ***A***, Cell viability was assessed 48 h post-transfection using an MTT assay. No significant cellular toxicity was detected at 50 and 100 ng of transfected PERK plasmids. Results were reported as the OD595 averaged ± standard error ($n = 3$; *$p < 0.05$; ****$p < 0.0001$, two-way ANOVA, Turkey's multiple comparisons). ***B***, Western blot analysis confirming that PERK and phosphorylated PERK were detectable when cells were transfected with 100 ng of transfected plasmid. The K622R mutation in PERK did not lead to phosphorylation validating the specificity of PERK activation.

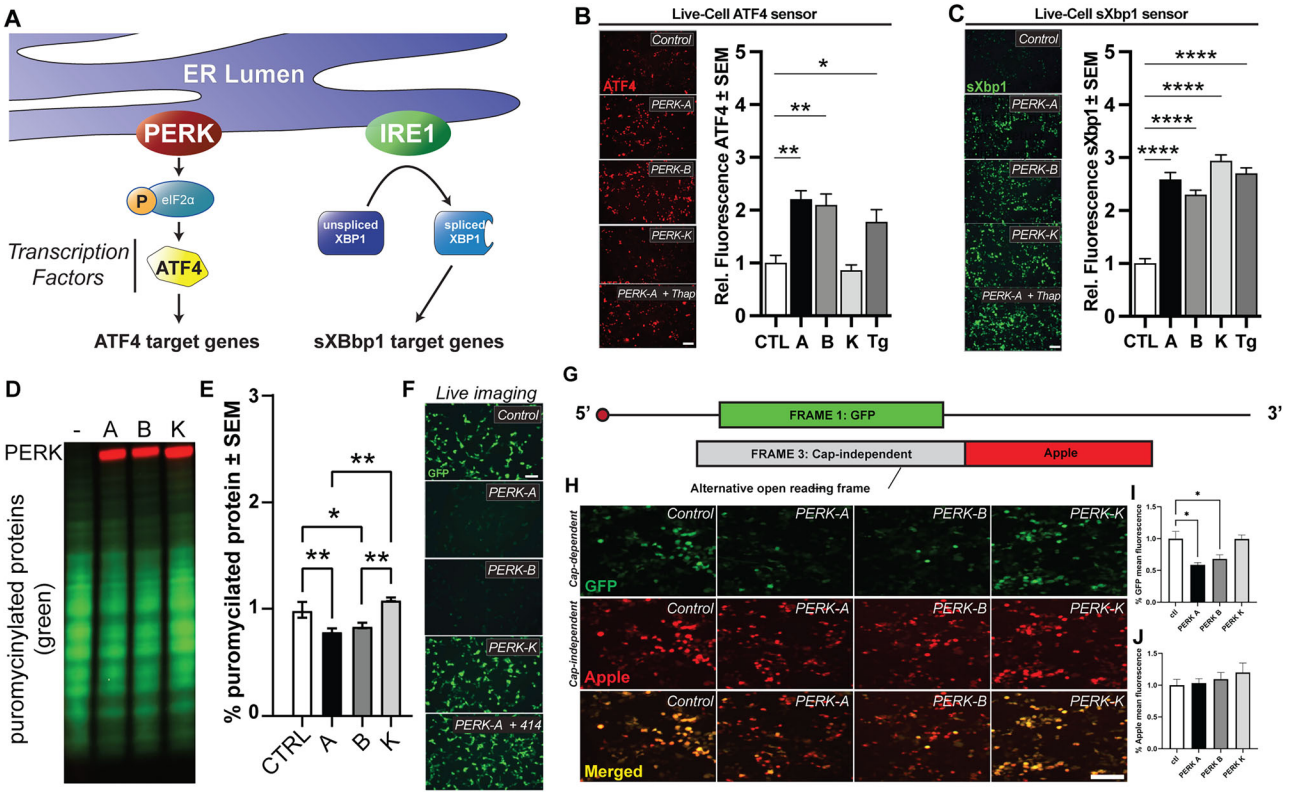

Figure 2. PERK-A and PERK-B canonical functions are indistinguishable. ***A***, Schematic representation of PERK and Ire1 activation leading to eIF2α phosphorylation and XBP1 mRNA splicing, key events in the UPR. ***B***, ***C***, PERK KO HEK293T cells were cotransfected with 100 ng of either an ATF4-mScarlet sensor (***B***) or an XBP1-mNeogreen sensor (***C***) along with 100 ng of PERK (PERK-A, PERK-B, or PERK-K) or an empty plasmid as a carrier. UPR activation was assessed by measuring fluorescence from the ATF4 and XBP1 sensors upon PERK expression or with thapsigargin (Tg) treatment. PERK-K expression also activated the XBP1 sensor. Relative fluorescence quantification shows significantly higher fluorescence levels for the activated sensors compared with controls ($n = 3$; $^*p < 0.05$; $^{**}p < 0.01$; $^{****}p < 0.0001$; one-way ANOVA, Dunnett's multiple comparisons). ***D***, ***E***, PERK KO HEK293T cells transfected with 100 ng of PERK constructs plus an empty plasmid were incubated with puromycin for 1 h. Western blot analysis shows reduced levels of puromycinylated proteins in cells expressing PERK-A or PERK-B, indicating repression of protein synthesis. Quantification of puromycinylated proteins is presented as mean ± SEM ($n = 3$; $^*p < 0.05$; $^{**}p < 0.01$; one-way ANOVA; Tukey's multiple comparisons). ***F***, Live imaging of PERK KO HEK293T cells transfected with 100 ng of PERK constructs and a GFP-expressing plasmid. Expression of PERK-A or PERK-B significantly reduced GFP fluorescence. The addition of a PERK inhibitor post-transfection reversed the PERK-A effect on GFP fluorescence. ***G***, Schematic representation of the GFP-Apple construct, where GFP is expressed in Frame 1 (cap-dependent) and Apple is expressed in Frame +3 (cap-independent) following the GFP stop codon. This design allows visualization of cap-independent translation through Apple fluorescence. ***H***, Live imaging of PERK KO HEK293T cells transfected with 100 ng of PERK constructs and the GFP-Apple plasmid. PERK-A and PERK-B expression reduced GFP fluorescence while allowing detectable Apple fluorescence, demonstrating selective repression of cap-dependent translation. ***I***, ***J***, Quantification of GFP fluorescence shows a significant reduction with PERK-A and PERK-B expression, while Apple fluorescence remains unaffected.

Compared to controls, total tau levels were reduced following transfection with either PERK-A or PERK-B, with no significant difference in total tau levels between the two variants (Fig. 3*B*,*D*, *E*). Under conditions of higher PERK expression (100 ng of cDNA for 48 h), total tau levels remained unchanged; however, PERK-B was less effective than PERK-A at reducing PHF1 levels (Fig. 3*B–D*). Similar differences were observed in other disease-associated phospho-tau species, including pS262 and pS202 (Fig. 3*F–H*).

Another important feature of tauopathies is deposition of insoluble tau species. To test the impact of PERK haplotypes on tau aggregation, we cotransfected PERK-A, PERK-B, or PERK-K with a tau variant that contains two disease-associated mutations (P301L and S320F) and is highly prone to aggregation (termed 2x Tau; Strang et al., 2018). We found that compared with PERK-A, PERK-B less effectively reduced insoluble tau (Fig. 4*A*,*B*). Therefore, while expression of both PERK haplotypes associated with reduced pathological tau species, PERK-B less competently decreased pathological tau, suggesting that longer overexpression of PERK-B leads to accumulation of pathological tau species compared with PERK-A. We corroborated these results using SH-SY5Y human neuroblastoma cells (Fig. S2).

PERK-A and PERK-B transcriptomes are similar, but their translatomes are unique

To establish differences in PERK-A and PERK-B that could explain how they differentially affect tau, we investigated changes in the transcriptome and the translatome. Our RNAseq experiments revealed stark differences resulting from PERK activation compared with control (Fig. S3); however, there were no significant differences in the transcriptome between the haplotypes.

PERK's canonical substrate, eIF2α, reduces overall translation while promoting the synthesis of unique RNA sequences with upstream open reading frames. To identify whether the differences between PERK-A and PERK-B resided in their corresponding translatomes, we coupled SUnSET with puromycin immunoprecipitation and liquid chromatography/tandem mass spectrometry (LC-MS/MS).

We identified distinct translatomes for each sample: control, PERK-A, and PERK-B. We found that 46% of the PERK-A translatome was unique compared with control and PERK-B (Fig. 5).

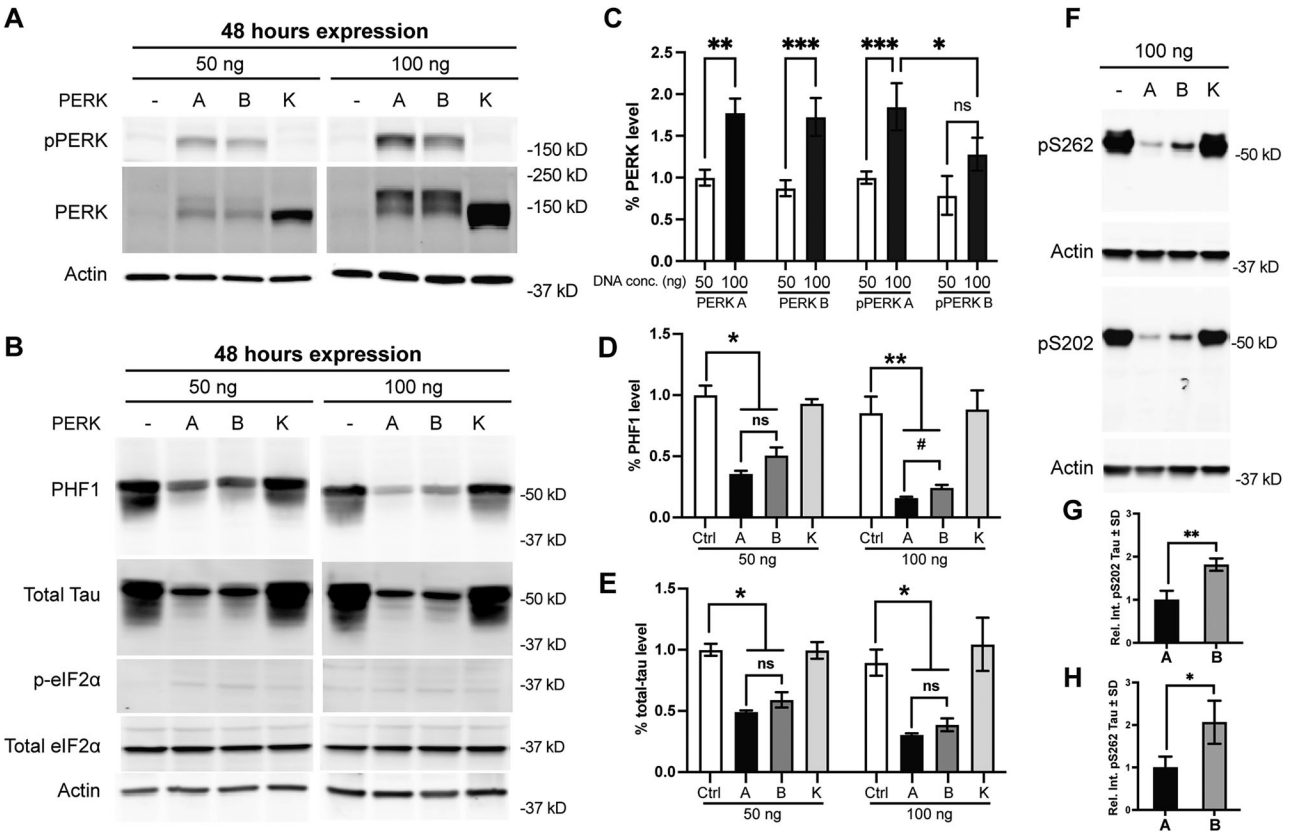

Figure 3. PERK-A expression reduces tauopathy-associated tau species more efficiently than PERK-B. PERK KO HEK293T cells were cotransfected with either 50 or 100 ng of PERK constructs (PERK-A, PERK-B; referred to as PERK-stress), along with an empty plasmid and 1 µg of a plasmid expressing human 0N4R tau. Cells were lysed 48 h post-transfection, and proteins were analyzed by Western blot and quantified by optical density. ***A***, ***B***, Transfection with 100 ng of PERK-A or PERK-B resulted in higher PERK expression compared with 50 ng. PERK-A showed a significant increase in phosphorylation at Thr982 when comparing 100 versus 50 ng, while PERK-B phosphorylation at Thr982 was not significantly higher at 100 ng and remained significantly lower than PERK-A at 100 ng. Optical density data are presented as percentage mean ± SEM ($n = 3$; ns, not significant; $^{*}p < 0.05$; $^{**}p < 0.01$; $^{***}p < 0.001$; two-way ANOVA; Tukey's multiple comparisons). ***C–E***, Expression of PERK-A or PERK-B at both 50 and 100 ng reduced PHF1 and total tau levels compared with the nonstressed control. PERK-A showed lower PHF1 levels compared with PERK-B when transfected at 100 ng ($^{*}p < 0.05$; $^{\#}p < 0.01$; two-tailed paired t test). Very low levels of phosphorylated eIF2α were detected under nonstress or PERK-stress conditions. ***F–H***, Western blot analysis of additional phospho-tau species (using the same samples from ***A***) shows that PERK-A compared with PERK-B led to lower levels of tau pS262 and pS202. Optical density data are presented as the percentage of the mean ± SEM ($n = 3$; $^{*}p < 0.05$; $^{**}p < 0.01$; two-tailed paired t test).

Meanwhile, only 2% of the PERK-B translatome was distinct from the other groups, suggesting that the risk imparted by PERK-B to develop PSP and AD is accounted within the 2% of nascently translated proteins. The PERK-A translatome exhibited an enrichment of proteins that suppress translation, as anticipated (Fig. S4). While PERK-B–expressing cells shared some overall features of this translatome, the effect was significantly less pronounced compared with the profile observed in PERK-A cells. We identified and compared differentially expressed proteins (Fig. S5) and found minor changes; PERK-B expression only reduced translation of the described transcripts. When listing the genes that were exclusively identified in each group, we found that only four proteins were uniquely identified in the PERK-B translatome: proteasome subunit alpha type-3 (PSMA3), alcohol dehydrogenase 5 (ADH5), distal-less homeobox 1 (DLX1), and neuroepithelial cell transforming gene 1 (NET1). Of these, only DLX1 was previously associated with PSP (Weber et al., 2018; Table 1, Fig. 5).

To corroborate that DLX1 levels are altered in PSP, we measured changes in the accumulation of DLX1 in the soluble and insoluble fractions of human PSP striatum (Fig. 6). As expected, PHF1 tau levels were significantly increased in PSP brains (Fig. 6*A*). DLX1 levels were increased only in the detergent-insoluble fraction; the soluble fraction had decreased DLX1 (Fig. 6*B–E*), suggesting a role of DLX1 redistribution in pathological processes in tauopathies.

To investigate the effects of DLX1 in vivo, we used a *Drosophila* model of tauopathy in which tau overexpression in the eye leads to severe retinal disorganization and reduced eye size (Fig. 7). When the fly DLX1 homolog, distal-less (*Dll*), was silenced in control flies (Fig. S6, 75% knock-down), there was no change in eye morphology (Fig. 7*A*). Tau-overexpressing flies showed significant alterations to eye morphology when coexpressed with the control Luciferase RNAi transgene (Fig. 7*B*). However, 75% knock-down of *Dll* in tau-overexpressing flies significantly rescued the eye defects (Fig. 7*C–E*), suggesting that DLX1 contributes to tau-mediated toxicity. To assess the effect in neuronal context, we conditionally expressed tau with Luciferase RNAi or *Dll* RNAi transgenes in the adult fly brain using the mushroom body GeneSwitch driver and found reduction of total tau levels upon Dll knock-down (Fig. 7*F*,*G*). Notably, *Dll* silencing had no effect on eye phenotypes induced by $A\beta_{42}$ (Fig. 7*H*,*I*), highlighting the specificity of the DLX1-tau effects over Aβ.

Discussion

We describe a novel mammalian cell culture system that enables PERK expression at levels that induce the UPR without the addition of toxic chemical compounds such as thapsigargin or

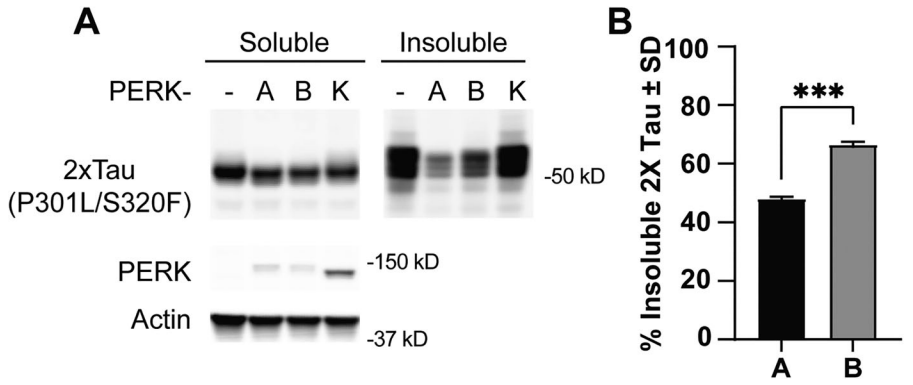

Figure 4. PERK-A expression reduces aggregation-prone 2x Tau (P301L/S320F) more efficiently than PERK-B. PERK KO HEK293T cells were cotransfected with 100 ng of PERK constructs (PERK-A, PERK-B, and PERK-K) or with an empty plasmid and 1 µg of 0N4R 2x Tau (P301L/S320F). Cells were lysed 48 h post-transfection and subjected to ultracentrifugation to separate detergent-soluble and detergent-insoluble fractions. ***A***, Both fractions were analyzed by Western blot and quantified by optical density. ***B***, The PSP variant PERK-B resulted in a significantly higher percentage of aggregated (insoluble) 2x Tau compared with PERK-A. Optical density data are presented as the percentage of insoluble tau ± SEM ($n = 3$; *$p < 0.05$; **$p < 0.01$; two-tailed paired t test).

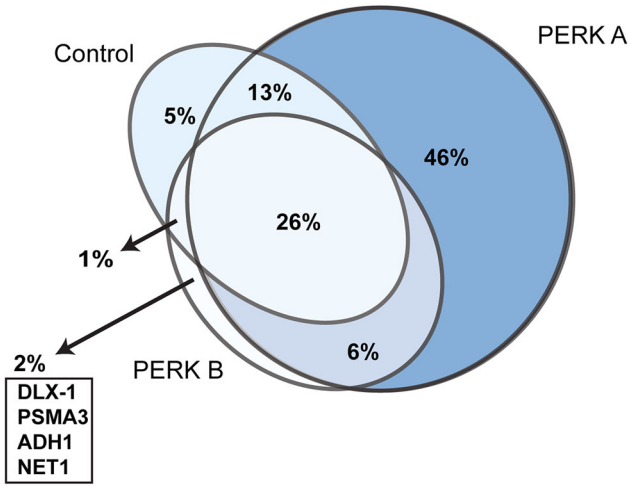

Figure 5. Expression of PERK-A or PERK-B alters global protein translation in vitro. PERK KO HEK293T cells were transfected with 400 ng of PERK constructs (PERK-A or PERK-B) along with an empty plasmid (control) in 10 cm dishes. At 48 h post-transfection, cells were incubated with puromycin (10 µg/ml) for 1 h to label nascent peptides. Protein lysates were collected and subjected to immunoprecipitation of puromycinylated peptides, followed by mass spectrometry analysis. Venn diagram shows the percentage of overlapping and unique peptides detected in each condition.

Table 1. Proteins identified in the PERK-B translatome but not in the PERK-A translatome

Protein	−log10 (p value)	Associated with PSP or AD
ADH5	1.98	No
NET1	1.66	No
DLX1	1.54	Weber et al. (2018)
PSMA3	1.51	No

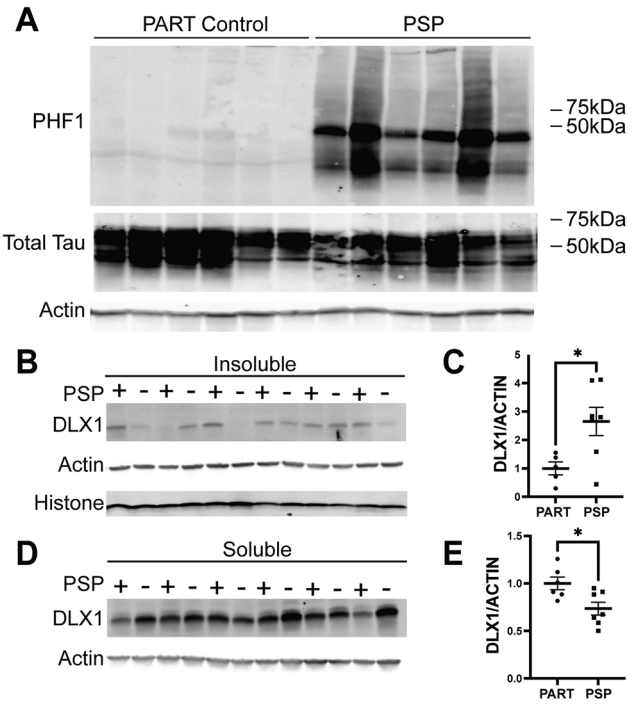

Figure 6. Human PSP brains present more insoluble DLX1. The striatum from PSP and early-stage primary age-related tauopathy (PART) human brains were processed to yield detergent-insoluble and detergent-soluble fractions. ***A***, PSP striatum samples contain significantly more PHF1 tau compared with early-stage PART controls. DLX1 is significantly increased in the (***B***, ***C***) detergent-insoluble fractions and significantly decreased in the (***E***, ***F***) detergent-soluble fractions. Actin and histone protein was used as control. Optical density data are presented as the percentage of DLX1/actin ± SEM ($n = 7–8$; *$p < 0.05$, two-tailed paired t test).

tunicamycin, and without inducing cell death. Using this system, we analyzed the impact of rare polymorphisms in the PERK gene that distinguish the A and B alleles on known PERK functions, including its broad suppression of translation. We established that canonical PERK functions were indistinguishable between the two variants. We observed no significant difference between PERK-A and PERK-B in the activation of ATF4 and sXBP1 transcription factors. PERK-A and PERK-B showed similar capacities to inhibit cap-dependent translation. As previously described, PERK activation diminished phospho-tau levels, but PERK-B was slightly less effective than PERK-A at reducing pTau epitopes we evaluated, confirming that this new model was consistent with previous systems (Harding et al., 2000b; Bruch et al., 2017). PERK-B was also less effective in preventing the aggregation of mutant tau P301L/S320F; these results were corroborated in SH-SY5Y human neuroblastoma cell model (Fig. S2). Utilizing this unique model in conjunction with puromycin-based proteomics, we uncovered a highly specific subset of proteins (comprising

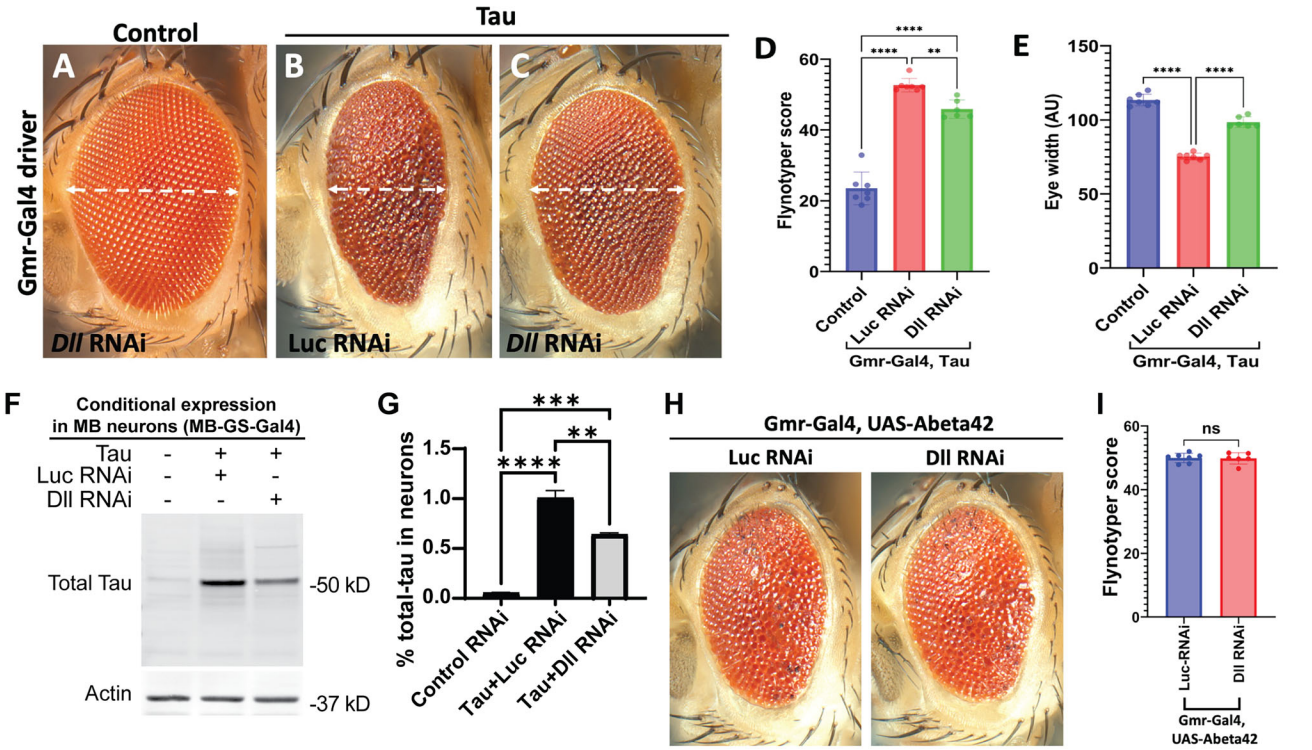

Figure 7. Distal-less/DLX1 silencing reduces tau toxicity in vivo. Representative eye images from *Drosophila* expressing either *Dll* RNAi alone (***A***), UAS-Tau with the innocuous Luciferase (Luc) RNAi control line (***B***), or UAS-Tau with *Dll* RNAi (***C***), under control of the eye-specific Gmr-Gal4 driver. Quantifications of the Flynotyper score (***D***) and eye width (***E***) are shown in arbitrary units (AU). The white dashed lines indicate maximum horizontal eye width measured with ImageJ ($n \geq 7$). Error bars indicate SEM. Statistical significance was determined by one-way ANOVA with Tukey's post hoc test. $^{**}p < 0.01$; $^{****}p < 0.0001$. ***F***, Representative Western blot showing total tau levels in brain homogenates from flies expressing UAS-Tau with either an innocuous Luciferase (Luc) RNAi control or *Dll* RNAi under control of the mushroom body GeneSwitch driver (MB-GS-Gal4). Flies were treated with RU486 (100 µg/ml) for 5 d to ensure robust and specific expression in the adult mushroom body neurons. ***G***, Quantification of panel ***F*** showing significantly reduced tau levels when *Dll* expression is knocked-down. Data are presented as percentage total tau normalized to actin, shown as mean ± SEM ($^{**}p < 0.01$; $^{***}p < 0.001$; $^{****}p < 0.0001$; one-way ANOVA with Tukey's multiple comparisons test). ***H***, Representative images of adult *Drosophila* eyes coexpressing the indicated transgenes under control of the eye-specific Gmr-Gal4 driver. ***I***, Quantification shows that flies coexpressing $A\beta_{42}$ and the Luciferase (Luc) RNAi control show similar phenotypes to flies coexpressing $A\beta_{42}$ and *Dll* RNAi, indicating no modification of $A\beta_{42}$ toxicity by *Dll* silencing. *T* test; ns, not significant.

only 2% of the total PSP-associated proteome compared with controls) that are differentially regulated by PERK-A versus PERK-B. Among the identified genes, DLX1 stood out as a driver of toxicity in mammalian cell culture. We also show that DLX1 is increased in insoluble fractions from human PSP brains and that reducing the *Drosophila* homolog of DLX1 in fly eye mitigates degeneration caused by the overexpression of WT human tau. Thus, our data link, for the first time, a toxic PERK–DLX1 pathway with tauopathy in human disease.

Increased activation of PERK correlates with tau pathology in PSP and AD brains (Stutzbach et al., 2013). We confirmed that beyond this positive correlation, PERK haplotypes differentially regulate tau and phospho-tau protein levels. However, Stutzbach and colleagues showed that immunoreactivity for active PERK and tau do not overlap in all cells. In addition, increased pPERK was detected in neurons lacking neurofibrillary tangles in brains from AD cases (Hoozemans et al., 2009). Therefore, it is important to determine whether expression of PERK haplotypes is cell specific, which is likely given results from previous work showing that astrocytic and neuronal PERK promote different UPR outcomes (Wolzak et al., 2022; Chen et al., 2025). Nonetheless, our data suggest that PERK-B–expressing cells have increased insoluble tau accumulation.

The PERK-B haplotype confers higher sensitivity to ER stress, inefficiently regulates eIF2α, has limited self-activation, and promotes accumulation of pathological tau (Liu et al., 2012; Stutzbach et al., 2013; Yuan et al., 2018). All these are mechanisms by which PERK-B carriers may have a higher risk for neurodegenerative diseases (Stutzbach et al., 2013). However, until now, these PERK mechanisms did not link the transcription factor DLX1 in a proteotoxic pathway with tau. We identified a highly specific PERK-B translatome (Table 1) that corresponds to only 2% of all proteins unique to PERK-B compared with control (nonstressed) and PERK-A (Tables 2, 3). DLX1 was the only protein identified that had been previously associated with PSP. Additional work is needed to evaluate whether the other PERK-B–associated proteins may impact tau directly and/or

Table 2. Proteins identified in the PERK-A translatome but not in the PERK-B translatome

Protein	−log10 (*p* value)
CC2DB	2.98
GIPC2	1.98
SF3A2	1.87
IPO5	1.87
ATP2A2	1.83
PDE4DIP	1.81
RBM15B	1.70
SP110	1.61
DNAJC7	1.56
AKR1B1	1.44

Table 3. Proteins identified in the PERK-A translatome but not in the control translatome

Protein	−log10 (*p* value)
MRPL10	5.72
MSX2	4.58
APOB	4.55
SNRNP70	4.39
THBS1	4.24
E2F7	3.23
NOP56	1.39
MRPL10	5.72
MSX2	4.58
APOB	4.55

play a role in PSP. Specific efforts could focus on whether PSMA3, ADH5, and NET1 also modulate pathological tau accumulation, contribute to indirect pathways (like PKR protein), are distributed in main brain regions affected in tauopathies, or exert control over protein regulation (via the proteasome, autophagy, and enzymatic activity). Our study identifies DLX1 as a key protein that influences tau toxicity in multiple systems, and it is strongly supported by previous work from Weber et al. genetically implicating DLX1 in PSP (Weber et al., 2018). Further research is required to address the precise mechanisms through which DLX1 modulates tau phosphorylation and aggregation.

PERK-B inefficiency to control tau levels can be explained by its limited self-phosphorylation and reduced kinase activity, which can lead to weak eIF2α activation after stress induction (Yuan et al., 2018). Because tau levels increase with age, correlating with declined proteostasis (Klaips et al., 2018), delayed and partial PERK-B activation over time can be detrimental for cells to cope with age-related cellular stress. Certainly, unregulated protein synthesis has the potential to create dyshomeostasis possibly contributing to cell death promoted by misfolded tau.

Our findings highlight the significant role that PERK haplotype variations play in shaping the cellular proteome in the context of PSP and draw greater attention to the importance of translational regulation pathways in neurodegenerative diseases. This PERK-associated translatome had not been previously associated with PSP, underscoring the novelty of these results and the opportunity it opens to unravel disease mechanisms.

Data Availability

The datasets and computer code produced in this study are available upon request.

References

Abisambra JF, et al. (2013) Tau accumulation activates the unfolded protein response by impairing endoplasmic reticulum-associated degradation. J Neurosci 33:9498–9507.

Aldrian D, et al. (2024) Natural history of Wolcott-Rallison syndrome: a systematic review and follow-up study. Liver Int 44:811–822.

Bell MC, Meier SE, Ingram AL, Abisambra JF (2016) PERK-opathies: an endoplasmic reticulum stress mechanism underlying neurodegeneration. Curr Alzheimer Res 13:150–163.

Bruch J, et al. (2017) PERK activation mitigates tau pathology in vitro and in vivo. EMBO Mol Med 9:371–384.

Casas-Tinto S, Zhang Y, Sanchez-Garcia J, Gomez-Velazquez M, Rincon-Limas DE, Fernandez-Funez P (2011) The ER stress factor XBP1s prevents amyloid-beta neurotoxicity. Hum Mol Genet 20:2144–2160.

Chen K, Morizawa YM, Nuriel T, Al-Dalahmah O, Xie Z, Yang G (2025) Selective removal of astrocytic PERK protects against glymphatic impairment and decreases toxic aggregation of β-amyloid and tau. Neuron 113: 2438–2454.e6.

da Silva DC, Valentao P, Andrade PB, Pereira DM (2020) Endoplasmic reticulum stress signaling in cancer and neurodegenerative disorders: tools and strategies to understand its complexity. Pharmacol Res 155:104702.

Ferrari R, et al. (2014) Assessment of common variability and expression quantitative trait loci for genome-wide associations for progressive supranuclear palsy. Neurobiol Aging 35:1514.e1–1514.e12.

Goodwin MS, et al. (2021) Anti-tau scFvs targeted to the cytoplasm or secretory pathway variably modify pathology and neurodegenerative phenotypes. Mol Ther 29:859–872.

Harding HP, Novoa I, Zhang Y, Zeng H, Wek R, Schapira M, Ron D (2000a) Regulated translation initiation controls stress-induced gene expression in mammalian cells. Mol Cell 6:1099–1108.

Harding HP, Zhang Y, Bertolotti A, Zeng H, Ron D (2000b) Perk is essential for translational regulation and cell survival during the unfolded protein response. Mol Cell 5:897–904.

Hoglinger GU, et al. (2011) Identification of common variants influencing risk of the tauopathy progressive supranuclear palsy. Nat Genet 43:699–705.

Hoozemans JJ, van Haastert ES, Nijholt DA, Rozemuller AJ, Eikelenboom P, Scheper W (2009) The unfolded protein response is activated in pretangle neurons in Alzheimer's disease hippocampus. Am J Pathol 174:1241–1251.

Kaufman RJ (2002) Orchestrating the unfolded protein response in health and disease. J Clin Invest 110:1389–1398.

Klaips CL, Jayaraj GG, Hartl FU (2018) Pathways of cellular proteostasis in aging and disease. J Cell Biol 217:51–63.

Kolberg L, Raudvere U, Kuzmin I, Adler P, Vilo J, Peterson H (2023) G: profiler-interoperable web service for functional enrichment analysis and gene identifier mapping (2023 update). Nucleic Acids Res 51: W207–W212.

Koren SA, Gillett DA, D'Alton SV, Hamm MJ, Abisambra JF (2019a) Proteomic techniques to examine neuronal translational dynamics. Int J Mol Sci 20:3524.

Koren SA, et al. (2019b) Tau drives translational selectivity by interacting with ribosomal proteins. Acta Neuropathol 137:571–583.

Koren SA, et al. (2021) Broad kinase inhibition mitigates early neuronal dysfunction in tauopathy. Int J Mol Sci 22:1186.

Lanzillotta C, Tramutola A, Meier S, Schmitt F, Barone E, Perluigi M, Di Domenico F, Abisambra JF (2018) Early and selective activation and subsequent alterations to the unfolded protein response in down syndrome mouse models. J Alzheimers Dis 62:347–359.

Lanzillotta C, et al. (2020) Chronic PERK induction promotes Alzheimer-like neuropathology in Down syndrome: insights for therapeutic intervention. Prog Neurobiol 196:101892.

Liu QY, Yu JT, Miao D, Ma XY, Wang HF, Wang W, Tan L (2013) An exploratory study on STX6, MOBP, MAPT, and EIF2AK3 and late-onset Alzheimer's disease. Neurobiol Aging 34:1519.e13–1519.e17.

Liu XA, Song J, Jiang Q, Wang Q, Tian Q, Wang JZ (2012) Expression of the hyperphosphorylated tau attenuates ER stress-induced apoptosis with upregulation of unfolded protein response. Apoptosis 17:1039–1049.

Marciniak SJ, Garcia-Bonilla L, Hu J, Harding HP, Ron D (2006) Activation-dependent substrate recruitment by the eukaryotic translation initiation factor 2 kinase PERK. J Cell Biol 172:201–209.

Meier S, Bell M, Lyons DN, Ingram A, Chen J, Gensel JC, Zhu H, Nelson PT, Abisambra JF (2015) Identification of novel tau interactions with endoplasmic reticulum proteins in Alzheimer's disease brain. J Alzheimers Dis 48:687–702.

Meier S, et al. (2016) Pathological tau promotes neuronal damage by impairing ribosomal function and decreasing protein synthesis. J Neurosci 36: 1001–1007.

Minjarez B, Calderon-Gonzalez KG, Rustarazo ML, Herrera-Aguirre ME, Labra-Barrios ML, Rincon-Limas DE, Del Pino MM, Mena R, Luna-Arias JP (2016) Identification of proteins that are differentially expressed in brains with Alzheimer's disease using iTRAQ labeling and tandem mass spectrometry. J Proteomics 139:103–121.

Moreno JA, et al. (2012) Sustained translational repression by eIF2alpha-P mediates prion neurodegeneration. Nature 485:507–511.

Moreno JA, et al. (2013) Oral treatment targeting the unfolded protein response prevents neurodegeneration and clinical disease in prion-infected mice. Sci Transl Med 5:206ra138.

Nijholt DA, van Haastert ES, Rozemuller AJ, Scheper W, Hoozemans JJ (2012) The unfolded protein response is associated with early tau pathology in the hippocampus of tauopathies. J Pathol 226:693–702.

Nougarede A, Tesniere C, Ylanko J, Rimokh R, Gillet G, Andrews DW (2018) Improved IRE1 and PERK pathway sensors for multiplex endoplasmic reticulum stress assay reveal stress response to nuclear dyes used for image segmentation. Assay Drug Dev Technol 16:350–360.

Ran FA, Hsu PD, Wright J, Agarwala V, Scott DA, Zhang F (2013) Genome engineering using the CRISPR-Cas9 system. Nat Protoc 8: 2281–2308.

Schmidt EK, Clavarino G, Ceppi M, Pierre P (2009) SUnSET, a nonradioactive method to monitor protein synthesis. Nat Methods 6:275–277.

Strang KH, Goodwin MS, Riffe C, Moore BD, Chakrabarty P, Levites Y, Golde TE, Giasson BI (2017) Generation and characterization of new monoclonal antibodies targeting the PHF1 and AT8 epitopes on human tau. Acta Neuropathol Commun 5:58.

Strang KH, Croft CL, Sorrentino ZA, Chakrabarty P, Golde TE, Giasson BI (2018) Distinct differences in prion-like seeding and aggregation between tau protein variants provide mechanistic insights into tauopathies. J Biol Chem 293:2408–2421.

Stutzbach LD, Xie SX, Naj AC, Albin R, Gilman S, PSP Genetics Study Group, Lee VM, Trojanowski JQ, Devlin B, Schellenberg GD (2013) The unfolded protein response is activated in disease-affected brain regions in progressive supranuclear palsy and Alzheimer's disease. Acta Neuropathol Commun 1:31.

Vanderperre B, Lucier JF, Bissonnette C, Motard J, Tremblay G, Vanderperre S, Wisztorski M, Salzet M, Boisvert FM, Roucou X (2013) Direct detection of alternative open reading frames translation products in human significantly expands the proteome. PLoS One 8:e70698.

Wang XZ, Kuroda M, Sok J, Batchvarova N, Kimmel R, Chung P, Zinszner H, Ron D (1998) Identification of novel stress-induced genes downstream of chop. EMBO J 17:3619–3630.

Waxman EA, Giasson BI (2010) A novel, high-efficiency cellular model of fibrillar alpha-synuclein inclusions and the examination of mutations that inhibit amyloid formation. J Neurochem 113:374–388.

Weber A, et al. (2018) Epigenome-wide DNA methylation profiling in progressive supranuclear palsy reveals major changes at DLX1. Nat Commun 9:2929.

Weihl CC, Dalal S, Pestronk A, Hanson PI (2006) Inclusion body myopathy-associated mutations in p97/VCP impair endoplasmic reticulum-associated degradation. Hum Mol Genet 15:189–199.

Wolzak K, Nolle A, Farina M, Abbink TE, van der Knaap MS, Verhage M, Scheper W (2022) Neuron-specific translational control shift ensures proteostatic resilience during ER stress. EMBO J 41:e110501.

Yuan SH, et al. (2018) Tauopathy-associated PERK alleles are functional hypomorphs that increase neuronal vulnerability to ER stress. Hum Mol Genet 27:3951–3963.